Journal of Infrared, Millimeter, and Terahertz Waves (2022) 43:349–365
https://doi.org/10.1007/s10762-022-00861-7

Resonant Atmospheric Plasma-Sprayed Ceramic Layers Effectively absorb Microwaves at 170 GHz

Andreas Hentrich[1] · Venancio Martinez Garcia[2] · Andreas Killinger[2] · Burkhard Plaum[1] · Carsten Lechte[1,2] · Günter E. M. Tovar[1]

Received: 8 February 2022 / Accepted: 13 June 2022 / Published online: 11 July 2022

Abstract

Microwave absorbing layer materials (MALMs) are extremely important for many components in fusion reactors to absorb microwave radiation in a controlled manner and with predictable power density. Therefore, a detailed knowledge of absorption properties of absorber coating materials used is necessary. Plasma-sprayed mixed oxide coatings are most commonly used in those applications where moderate power density is expected. In this paper, a plane wave absorption model is presented using refractive index and absorption coefficient as internal parameters and incidence angle, polarization, and layer thickness as external parameters. The model has been calculated assuming radiation of 170 GHz, as envisaged for the ITER research facility. Three atmospheric plasma-sprayed coating materials were considered in this work: titanium dioxide (TiO_2), chromium oxide (Cr_2O_3), and a mixed aluminum-titanium oxide Al_2O_3-TiO_2 (40/60). Theoretical results are compared with free wave measurements with two antennas. Different coating thicknesses have been prepared and measured in different polarization and incidence angles. Results are discussed regarding polarization, incidence angle, layer thickness, absorption coefficient, and refractive index.

Keywords Modeling · Experimental validation · Plasma spray coatings · Mixed oxides

✉ Andreas Hentrich
andreas.hentrich@igvp.uni-stuttgart.de

[1] Institut für Grenzflächenverfahrenstechnik und Plasmatechnologie, University of Stuttgart, Pfaffenwaldring 31, D-70569 Stuttgart, Germany

[2] Institut für Fertigungstechnologie keramischer Bauteile, University of Stuttgart, Allmandring 7b, D-70569 Stuttgart, Germany

1 Introduction

Microwave absorption materials are especially relevant in fusion research due to the massive energy which is required to start a fusion process. Small percentages of stray radiation can produce catastrophic effects on some components, even destroying the complete system. An ongoing field of research is to find materials, which can work under the aggressive conditions regarding radiation and heat inside a reactor as a reliable beam dump. The most important properties such a material needs to fulfill are as follows: resistance to high temperatures, vacuum compatibility, a reliable production process with reproducible parameters, and compactness, and obviously it also needs to absorb a high percentage of the incoming microwave radiation. While in the moment often carbon-based systems are used [1, 2], many of the possible candidates are ceramic layers, and three of these are presented in the paper: an aluminum oxide and titanium oxide compound material (Al_2O_3-TiO_2 (40/60)), chromium oxide (Cr_2O_3), and pure titanium oxide (TiO_2), with a focus on the compound material.

In this study, the frequency applied is 170 GHz due to the collaboration with the International Thermonuclear Experimental Reactor (ITER), whose purpose was to find possible beam dumps for the first plasma experiment [3]. This frequency also predetermines the thickness range of the samples. To obtain a high enough absorption, interference effects are used, which result in a resonant thickness. In particular with regard to DEMOnstration Power Plant class reactors (DEMO), which is the first planned nuclear fusion energy plant and the intended successor to ITER, it is necessary to examine the performance of possible beam dump candidates at higher frequencies than previously tested. In this study, it will be shown that some of the investigated oxide layers reliably have the absorption properties necessary for these purposes.

2 Model

The general theory of absorbing dielectric materials is well known [4] and several similar models have been proposed in similar situations. This goes from a single layer on a substrate considering a single reflection [5], over a layer system with a single passage [6], to a single absorbing layer considering both multiple reflections and transmission [7]. None of these describes the situation on hand sufficiently. Thereby, a model is proposed with the following corner stones: It is a single layer on a substrate, which acts as an almost perfect mirror; multiple reflections are considered; and the approximation for weak absorbing materials is not used.

A simple plane wave model was used to estimate the internal properties of the materials. Two internal parameters are expected to be relevant: the refractive index and an absorption coefficient. The other relevant parameters are all material independent and measurable: the incidence angle, the polarization, and the layer thickness.

The modeling (Fig. 1) starts with a simple plane wave hitting the surface of the layer material under a certain incidence angle ($A - L_0$). Depending on the polarization, the respective Fresnel formula is used. For these, the outgoing angle into the material is necessary, which would in most cases be calculated by Snell's law. This simplification is just valid for small absorptions or small conductivities though, which can not be assumed for the materials analyzed in this paper, when their purpose is to absorb high percentages. So instead, the wave vector needs to be derived from the Maxwell equations for linear isotropic mediums, taking into consideration the conductivity and a complex permittivity:

$$\Delta \mathbf{E} + k_{layer}^2 \mathbf{E} = 0 \tag{1}$$

$$k_{layer}^2 = \epsilon \mu \omega^2 - i \mu \omega \sigma \tag{2}$$

The following notation is used: k_{layer} is the wave vector inside the layer, i the imaginary unit, ϵ the complex permittivity, μ the permeability, ω the frequency, and σ the conductivity. For metals, the first term of the wave vector formula could be

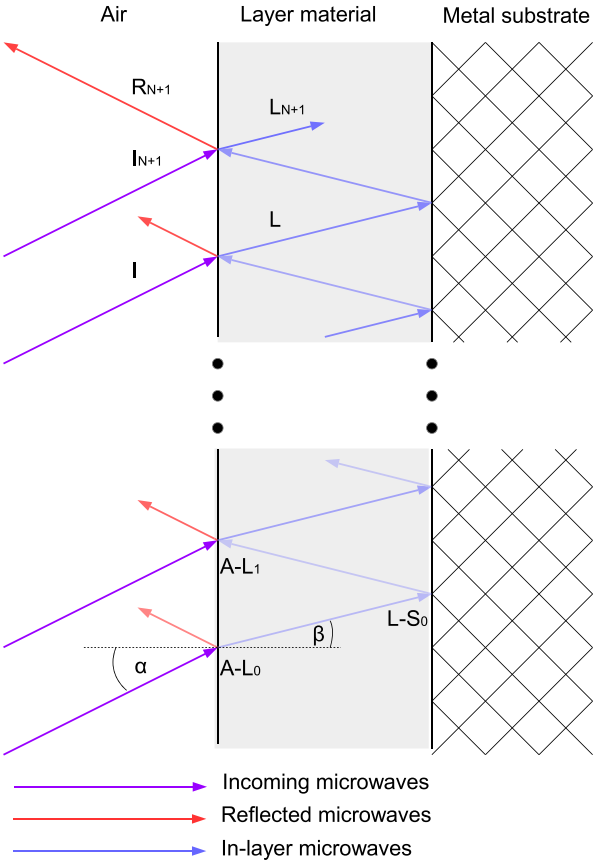

Fig. 1 Sketch for the Plane Wave Model

neglected, and for low absorbing materials the second one, which would vastly simplify the problem. Instead, we split the permittivity into real and imaginary parts and rearrange the formula to:

$$k_{layer}^2 = \epsilon' \mu \omega^2 - i\mu\omega(\omega\epsilon'' + \sigma) \tag{3}$$

The absorption has two contributions: one from the imaginary part of the refractive index and one from the conductivity. Therefore, a joint parameter is introduced for the expression inside the brackets, the aforementioned absorption coefficient $A_{layer} = \omega * \epsilon'' + \sigma$, because for a single-frequency model, the two contributions can not be distinguished. In addition, the frequency dependencies of σ and ϵ'' themselves will be neglected. Using $\epsilon'\mu = n_{layer}^2/c^2$ and $\omega = k_0 c$, with c being the vacuum light speed, k_0 the wave vector in air, and n_{layer} the real part of the refractive index inside the layer, the square root can be calculated leading to the following formula for k_{layer}:

$$k_{layer} = \sqrt{\frac{\sqrt{n_{layer}^4 k_0^4 + k_0^2 c^2 \mu_{layer}^2 A_{layer}^2} + n_{layer}^2 k_0^2}{2}} \tag{4}$$

With this wave vector and the boundary condition, that the wave vector parallel to the surface is identical inside and outside of the layer, the outgoing angle β can be calculated trigonometrically. With this information, the reflected and the transmitted parts can be calculated with the Fresnel formulas for both polarizations.

Simply taking this result to calculate the reflectivity of the layer would lead to a vastly inaccurate estimate in all cases but the ones with extremely high layer absorption or very large thickness because no multiple reflection was taken into account. To mitigate this flaw, the propagation of the transmitted part inside the layer is then calculated: Because both angle and wave vector are already known, the change in phase while passing through the layer is simple to calculate. For the amplitude, an exponential decay with A_{layer} as a parameter is assumed. Reaching the layer-substrate interface ($L - S_0$), the polarization must again be taken into account: When the electric field is perpendicular polarized with respect to the incidence plane, a phase shift of $\pi/2$ is added, in parallel polarization nothing is added.

Then another propagation through the layer follows, until the air-layer interface ($A - L_1$) is reached again. At this point, another part of the incoming plane wave also needs to be considered. This has a phase shift compared to the initial part of the incoming plane wave, simply because it moved an additional distance through air.

Both the incoming wave from outside the layer and the wave from inside the layer are now split into two parts with the Fresnel formulas. This results in four waves: the incoming will result in a transmitted part into the layer and one reflected back into the air, the wave from inside the layer will be split into one part transmitted into the air and one reflected back into the layer. Under consideration of the respective phases, the interference of the two waves outside the layer

is calculated, which is a slightly better estimate for the reflectivity of the layer system than just taking into account the first interface. Additionally, the interference of the waves inside the layer is calculated, with which the next iteration step can be calculated.

This results in the recursive set of formulas for the complex amplitudes:

$$L_{N+1} = L_N \cdot e^{\left(\frac{2\pi i}{\lambda_{mat}} - A_{layer}\right) \cdot \frac{2t}{cos(\beta)} \left(+\frac{\pi i}{2}\right)} \cdot R_I + I_N \cdot e^{4\pi i t \frac{tan(\beta)sin(\alpha)}{\lambda_{air}}} \cdot T_O \tag{5}$$

$$R_{N+1} = L_N \cdot e^{\left(\frac{2\pi i}{\lambda_{mat}} - A_{layer}\right) \cdot \frac{2t}{cos(\beta)} \left(+\frac{\pi i}{2}\right)} \cdot T_I + I_N \cdot e^{4\pi i t \frac{tan(\beta)sin(\alpha)}{\lambda_{air}} \left(+\frac{\pi i}{2}\right)} \cdot R_O \tag{6}$$

Here, L_N denotes the complex amplitude of the wave inside the layer after the N-th iteration, R_N the complex amplitude of the respective outgoing wave. The t is the thickness of the layer and λ_{mat} the wavelength inside the material. α is the incidence angle and β the angle between wave vector and the perpendicular inside the layer. The factors T_I, R_I, T_O, and R_O are the results of the Fresnel formulas, transmitted part from inside the layer, reflected from inside, transmitted from outside, and reflected from outside, respectively. These are dependent on the polarization; in the case of perpendicular polarized waves, also the $+\frac{\pi i}{2}$ are added.

After a few reflections, the reflected wave begins to converge against a certain value in both amplitude and phase. The square of the amplitude of the reflected wave divided by the square of the one of the incoming wave is now assumed to be the reflectivity of the layer material. The condition for convergence is reached when the difference in amplitudes of the reflected wave between two steps is below 0.1%. This is in most cases reached after less then 15 internal reflections, except for really high incoming angles or really low absorption coefficients, where it can take up to 100 reflections.

This algorithm can now be used to fit the measured data. Due to there being just two parameters in ranges that can be well assumed to be within certain thresholds, and the calculation time of a single point is negligible, a brute force alghorithm is fast and sufficient: At first, a sufficiently large parameter range is chosen for both the refractive index and the absorption coefficient, such that the sample parameters are for sure somewhere inside the range. Then, for every combination of parameters, the modeled reflectivity is calculated for every single measured thickness and angle of the material. Then the difference between model and measurement in every measurement point for every thickness t_x, angle α_y, and polarization p_z is calculated and then squared. The standard deviation $\sigma_{n,A}$ is the root of the sum of these squared differences divided by the number of measurements:

$$\sigma_{n,A} = \frac{\sqrt{\sum_{x,y,z=0}^{m,n,o} (R_{measured}(t_x, \alpha_y, p_z) - R_{modeled}(t_x, \alpha_y, p_z, n, A))^2}}{mno} \tag{7}$$

In this fashion, a standard deviation is associated to every combination of refractive index and absorption coefficient (compare Fig. 2).

The combination with the smallest standard deviation is then expected to be the closest to the real material parameters. To both save calculation time and increase

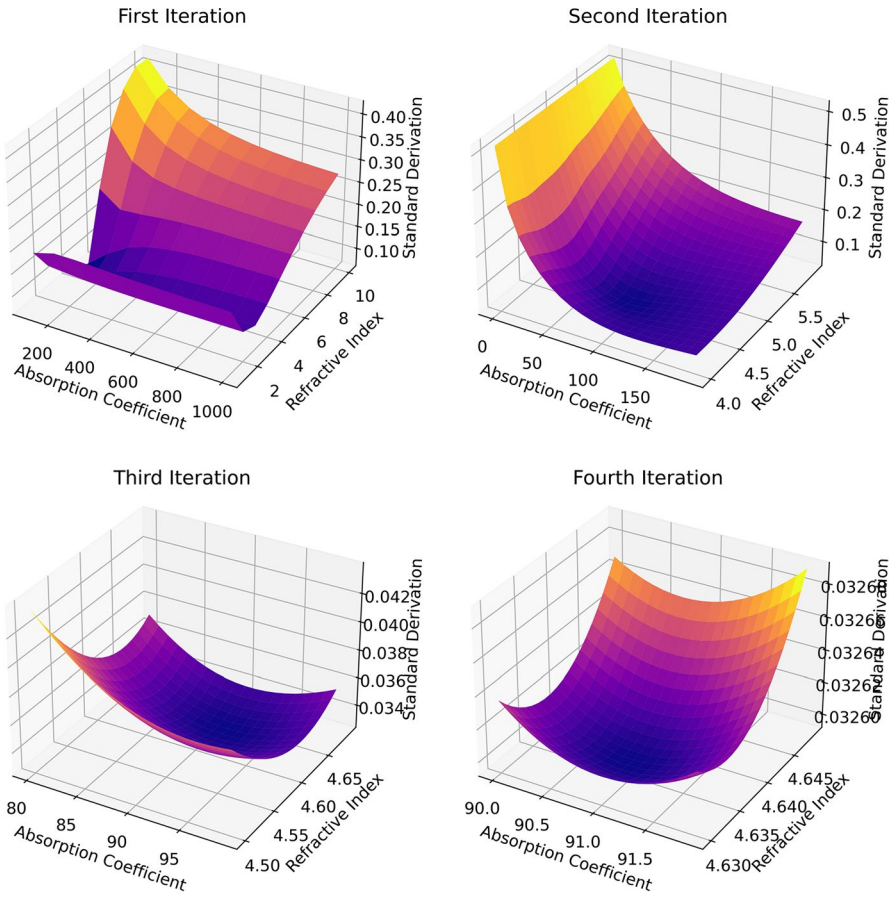

Fig. 2 Example of the fitting algorithm. In this case for Al_2O_3–TiO_2 (60/40). The standard deviation between measured and modeled data is shown for different combinations of internal parameters. The range of input parameters is a result of the respective previous iteration. In every iteration, a clear minimum can be found, which corresponds to a combination of absorption coefficient and refractive index, which is best suited to describe the material

accuracy, this algorithm is set up in an iterative way. Thereby after the first estimate of the combination is known, just the direct surrounding in parameter space is calculated in the next iteration by changing both range and step size.

3 Sample Preparation

The focus of this paper is on the Al_2O_3-TiO_2 compound material. There are two reasons for this: At first, this was the material system out of the three tested ones, which showed the best properties for the intended usage as a beam dump. Secondly, it was the material system directly produced at the Institut für

Fertigungstechnologie keramischer Bauteile (IFKB), whereby the production process was more replicable. The samples from the other two material systems were produced as a part of an ITER contract: The pure TiO_2 samples were produced by Metal Technology in Indiana (USA) and the Cr_2O_3 samples by Flame Spray in Milano (Italy). The respective thickness measurements were performed by the companies.

For the compound material, aluminum alloy 6061/82-T6 substrates were used with dimensions of 100mm * 100mm * 8mm. This substrate was grit blasted with corundum F60 and 3-bar air pressure to activate the surface before the coating process. This resulted in surface roughness parameters of $R_z = 32.99\ \mu$m and $R_a = 4.44\ \mu$m, which were measured by a contact profilometer type Perthometer Concept from Mahr GmbH (Germany) and were proven before [8] to be sufficient for the following plasma spraying. For this, an Al_2O_3-TiO_2 mixture spray powder of type Amdry 6250 was used, which was produced by Oerlikon Metco AG (Switzerland) with a composition of 60 % Al_2O_3 and 40 % TiO_2. The particle size distribution of the powder is given by the company as follows: D10, so the diameter where just 10% of the particles in the powder are smaller, is given as 5 μm and D90, where the diameter 90% of the particles are smaller, is given as 35 μm. This means the vast majority of the particles are between 5 and 35 μm. The atmospheric plasma spraying was performed using a standard F6 type plasma gun from GTV GmbH (Germany) guided by a six-axis robot system type RX130B from Stäubli International AG (Germany) and a PF962 powder feeder from GTV GmbH (Germany). To obtain a well adherent and dense coating structure with a thickness deposition of 10 to 20 μm per spray pass, the plasma parameters were adjusted accordingly (Fig. 3).

For the Al_2O_3-TiO_2 coatings in Table 1, the thickness was determined by non-destructive methods using a portable contact system DUALSCOPE®FMP100 coating thickness gauge from Helmut-Fischer GmbH (Germany), which uses the eddy current testing method (DIN EN ISO 2360) for non-ferrous metals.

Additionally, two samples were produced, one with 80 μm thickness and one with 120 μm, which were prepared to obtain cross-section images of the samples. The measurement of the coating thickness by non-destructive methods

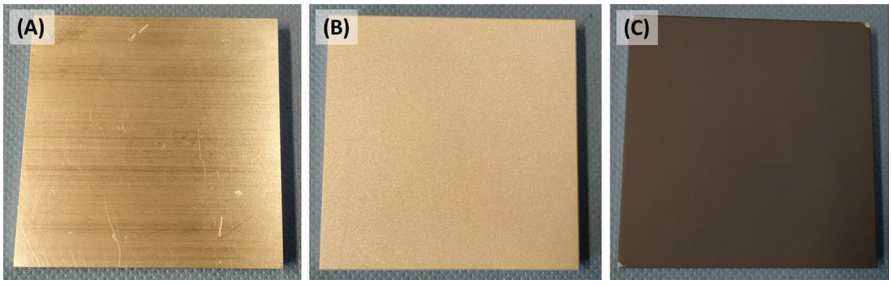

Fig. 3 The production process of the compound material. **A** shows the substrate, **B** the substrate after grit blasting, and **C** the finished sample after plasma spraying

Table 1 Sample list

Name	Layer material	Thickness (μm)	Error (μm)
TiO_2-1	Titanium dioxide	48.5	±15
TiO_2-2	Titanium dioxide	72.4	±15
TiO_2-3	Titanium dioxide	123.6	±25
TiO_2-4	Titanium dioxide	159.9	±25
TiO_2-5	Titanium dioxide	255.5	±6.2
Cr_2O_3-1	Chromium(III) oxide	54	±10
Cr_2O_3-2	Chromium(III) oxide	62	±10
Cr_2O_3-3	Chromium(III) oxide	82	±10
Cr_2O_3-4	Chromium(III) oxide	123	±13
Cr_2O_3-5	Chromium(III) oxide	139	±15
Cr_2O_3-6	Chromium(III) oxide	180	±15
Cr_2O_3-7	Chromium(III) oxide	201	±10
Cr_2O_3-8	Chromium(III) oxide	227	±15
Al_2O_3-TiO_2-1	60 % Al_2O_3, 40 % TiO_2	30.5	±2.3
Al_2O_3-TiO_2-2	60 % Al_2O_3, 40 % TiO_2	39.3	±2.3
Al_2O_3-TiO_2-3	60 % Al_2O_3, 40 % TiO_2	57.4	±2.1
Al_2O_3-TiO_2-4	60 % Al_2O_3, 40 % TiO_2	77.3	±3.8
Al_2O_3-TiO_2-5	60 % Al_2O_3, 40 % TiO_2	87.5	±3.1
Al_2O_3-TiO_2-6	60 % Al_2O_3, 40 % TiO_2	88.2	±3
Al_2O_3-TiO_2-7	60 % Al_2O_3, 40 % TiO_2	100.5	±4.6
Al_2O_3-TiO_2-8	60 % Al_2O_3, 40 % TiO_2	105.7	±4.4
Al_2O_3-TiO_2-9	60 % Al_2O_3, 40 % TiO_2	114.3	±4.4
Al_2O_3-TiO_2-10	60 % Al_2O_3, 40 % TiO_2	120.8	±3.56
Al_2O_3-TiO_2-11	60 % Al_2O_3, 40 % TiO_2	178.1	±3.5

A list of the samples used for the reflectivity measurements. The error column corresponds for the TiO_2 and the Cr_2O_3 to the values given by the respective producers, for the Al_2O_3-TiO_2 to the standard deviation of the thickness measurement

could be validated by metallographic cross-section thickness analysis, which also allowed analyzing the internal structure of the layer material (Fig. 4).

As can be seen in the figure, the material has an inhomogeneous internal structure, and Al_2O_3 (dark gray) zones and TiO_2 (light gray) zones are easily distinguishable. The interface between the coating and substrate is typical for atmospheric plasma spray coatings, which provides a good mechanical connection and thereby improving the adhesion strength.

The second destructive method used was the pull-off method ISO 14916 to measure this adhesion strength. For the measurement, an universal testing machine Zwick Z100 from ZwickRoell GmbH & Co. KG (Germany) was used, the adhesive was HTK ULTRA BOND® from HTK Hamburg GmbH (Germany) and as tension rod pins with a diameter of 14.2 mm were used. The glue was

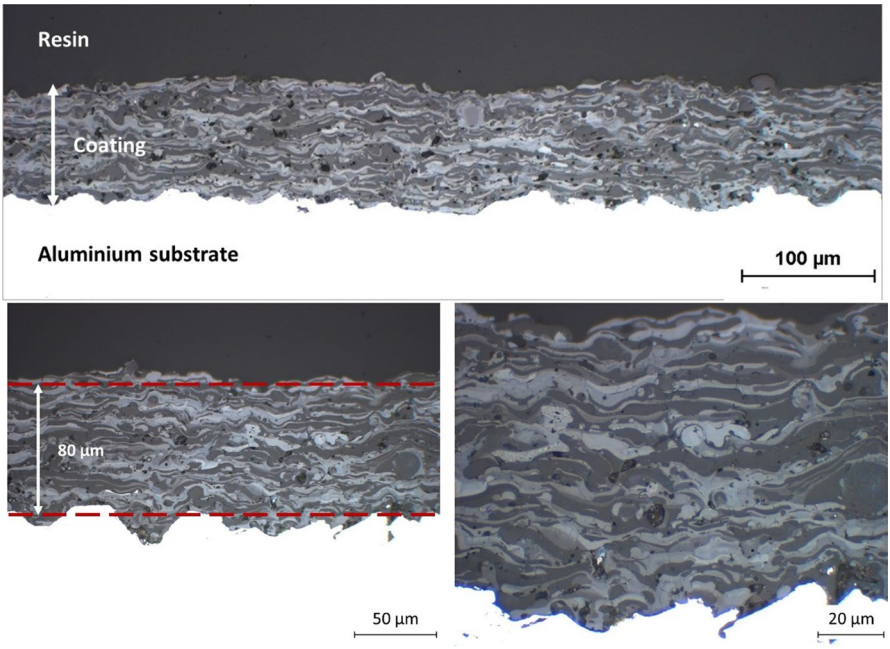

Fig. 4 The cross section of a layer of the Al_2O_3-TiO_2 compound material in different magnifications

heat treated with 190°C for 35 min and the test speed 0.5 mm/min. An adhesion strength of 8.45 ± 1.24 MPa was obtained, which is an expected value.

4 DC Characterization

As described in Section "2," the absorption coefficient is composed of two contributions: the imaginary part of the reflective index and the conductivity. It is advantageous to know if one of these contributions dominates the behavior or if both are equally relevant. The conductivity can be measured by the four-point probe

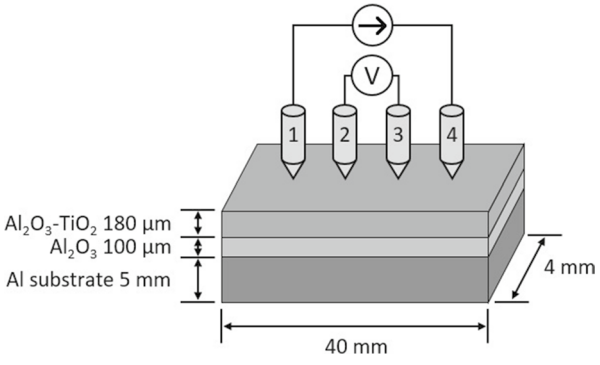

Fig. 5 Sketch of the four-point method and the measured sample

technique: four equally spaced (13.5 mm) co-linear probes are brought into contact of Al_2O_3-TiO_2 compound material sample with 180-μm thickness. To isolate the sample from the highly conductive aluminum substrate, a layer of pure Al_2O_3 with a thickness of 100 μm was plasma sprayed in between (compare Fig. 5). A known DC current is applied between the outer probes and the resulting voltage between the inner probes is measured. The resistivity is calculated considering different factors, such as geometry, the source current, and the voltage measurement [9]. The setup was self-built using a Multimeter Keithley 2750 from Keithley Instruments, Inc. (Cleveland, USA).

A sheet resistance of $2251 \pm 55 \frac{\Omega}{m}$ was obtained; by taking this value times the thickness, it is possible to calculate the resistivity. This leads to a resistivity of $0.405 \pm 0.010\ \Omega m$, which is equivalent to a conductivity of $2.269 \pm 0.057 \frac{S}{m}$. Comparing this with a similar sample from literature [10], an 87% Al_2O_3 - 13% TiO_2 coating produced by APS materials with a thickness of 400μm on which polarization tests on a three-electrode cell were performed, an average charge transfer resistance of $18{,}062 \pm 439\ \Omega$ was found. The difference will most likely result from the different material composition.

5 Measurement Procedure

For the reflectivity measurements, a vector network analyzer (Fig. 6) and two antennas are used. The incident wave is transmitted with a horn antenna through a mirror set up onto the sample. The reflected part will reach another horn antenna, the receiving one.

The measurements themselves were performed as followed: To ensure thermal stability of the setup, for 1.5 h before starting an actual measurement, a dummy measurement is performed. Then, at first a frequency sweep of a reference sample, an aluminum disk assumed to have ideal reflection, was measured under all

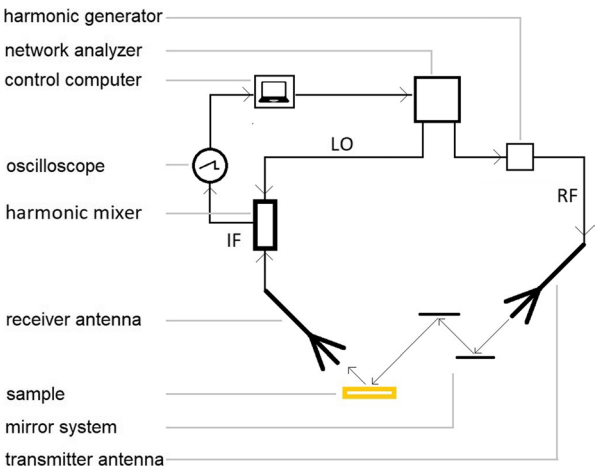

Fig. 6 The setup for the reflectivity measurements. The arrows symbolize the signal pathway; the additional mirrors are for focussing. The network analyzer generates two slightly different waves. With the first one, the radio fequency (RF) is generated, which is interacting with the sample and then fed into the harmonic mixer. The second one, the local oscillator (LO), is directly sent to the harmonic mixer to generate together with the RF the intermediate frequency (IF), which then can be measured

incidence angles, afterwards one of the first sample. The frequency sweep allows later in the analysis to exclude the effects of standing waves due to internal reflection in the setup. The reference measurement is repeated after each sample; this lowers the likelihood of problems with the measurements occurring unnoticed. When all samples are measured, the polarization is changed before repeating the procedure. The reference data is then scanned for aforementioned problems, and when none is abundant, the analysis starts.

For this, the frequency range is chosen in such a small range, from 169.5 to 170.5 GHz, that the reflectivity of both sample and reference should not change significantly. Indeed, they do not, except for a sinusoidal dependency of the frequency due to the standing waves. This issue is resolved by averaging over the standing wave. This value is considered to be the correct linearized signal under exclusion of internal reflections. The reflectivity is then simply the linearized signal of the sample divided by the mean of the linearized signal of the reference sample measurements with the same polarization and incidence angle.

Due to there being more than one reference sample measurement, some analysis can be made to give an estimate of the expected standard deviation of the measurement, which was in all cases below 8%. The standard deviation itself is slightly misleading as an error though the division of two possibly error containing values will make sure of that. When assuming that the percentage of deviation is mostly constant for both values, the high and low estimates of the reflectivities can be given as:

$$r_{high/low} = \frac{S_{Sample}(100 \pm Std)}{S_{Reference}(100 \mp Std)} \tag{8}$$

with Std being the standard deviation in percent, S_{Sample} the linearized signal of measurement of the sample, and $S_{Reference}$ the linearized signal of the reference. This error estimate also indicates an important restriction of the measurements: When the measured sample has a high reflectivity, S_{Sample} and $S_{Reference}$ are very similar, which vastly increases the possible resulting error in reflectivity. This makes measurements of reflectivities above 70–80% notoriously unreliable and especially sensitive to measurement problems.

6 Results

The results of both the modeling and the measurement can be seen in Fig. 7, and the respective parameters for the fits are given in Table 2.

A strong resonator effect was observed both in model and experiment. This resonator effect is caused by a negative interference between microwaves, which are reflected at the air-layer interface, and ones reflected at the layer-metal interface, which leads to a much enhanced distance the energy takes through the layer. For this to occur, the thickness and refractive index of the layer need to lead to a phase shift equal to $(2n + 1)\pi, n \in N^*$.

The three materials are good examples for different regions in the range of absorption coefficients: To start at one end of the range, TiO_2 (Fig. 7a and b) has

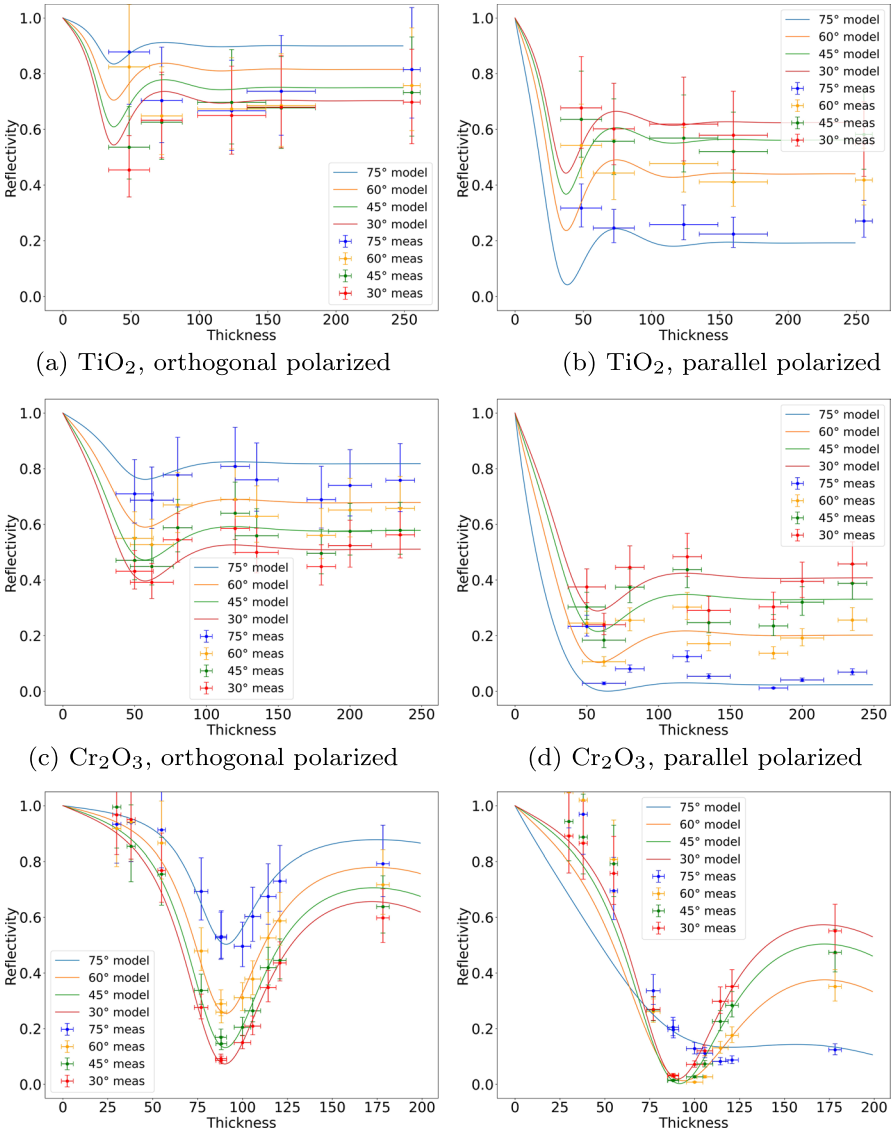

(a) TiO_2, orthogonal polarized (b) TiO_2, parallel polarized

(c) Cr_2O_3, orthogonal polarized (d) Cr_2O_3, parallel polarized

(e) Al_2O_3-TiO_2 , orthogonal polarized (f) Al_2O_3-TiO_2 , parallel polarized

Fig. 7 The measured data (dots) compared to the modeled thickness dependency (line)

a very big absorption coefficient. Thereby almost all of the energy that the microwave carries into the sample is dissipated into heat almost immediately. This both strongly decreases the Q-factor and thereby the resonator properties of the layer and increases the importance of the first air-layer interface. Additionally, the reflectivity becomes mostly independent of the thickness above a certain value. For the

Table 2 Resulting parameters

Material	Refractive index	Absorption coefficient	Error (± %)
TiO_2	9.845	>1000	6.42
Cr_2O_3	5.216	545.8	4.77
Al_2O_3-TiO_2	4.734	93.3	6.68

modeling, it becomes impossible to give an accurate estimate for the absorption coefficient, thereby just a lower limit for the absorption coefficient of TiO_2 is given.

With a slightly lower absorption coefficient, the thickness dependency becomes similar to the one of Cr_2O_3 (Fig. 7c and d): While the reflectivity is clearly not independent anymore of the thickness, the resonator property and thereby the thickness dependency is still partially suppressed. At around 55μm and to a lesser extent at the expected 165μm, two drops of reflectivity (or equivalent: peaks of absorption) can be observed in both polarizations . Like in both other materials, the orthogonal polarization has a significantly higher reflectivity than the parallel one.

When the absorption coefficient of the sample has an even more moderate value, the lowest in this study, a thickness dependency comparable to the one of Al_2O_3-TiO_2 (Fig. 7e and f) is observed: The peak in absorption is now very distinct and will reach values close to 100%, especially for small incidence angles. At the same time, compared to the thickness dependency of Cr_2O_3, the reflectivity between two peaks of absorption, so around 180μm, is higher. In the figures just the first absorption peak is visible, and the next is predicted by the model to be around 280μm and thereby out of the range of measured samples. This behavior also can be explained with the model: Between the resonances, an increase of the absorption coefficient obviously directly increases the complete absorption of the layer.

The angular dependency (Fig. 8) shows a clear trend, with the exception of really small thicknesses (<40 μm), where both the production and the measurement setup reach their limits. For high incidence angles, microwaves with orthogonal polarization are reflected at a much higher percentage than the microwaves with parallel polarization. The closer the incidence angle gets to 0, the smaller the difference between both polarizations becomes. This is simply due to the fact that at perpendicular incidence, there is no unambiguous plane of incidence anymore, so the polarizations become indistinguishable.

The suppression of the thickness dependency by high absorption coefficients can also be seen in these graphs, when comparing the results with the respective calculated limit of thickness against infinity, which is identical with just taking into account the first air-layer interface. While above a thickness of 120 μm the measurement and the high thickness limit are in all cases almost identical, the measurements below this thickness just vary strongly for the sample with the low absorption coefficient.

Additionally, a conclusion can be drawn if the contribution of the conductivity or the one of the imaginary part of the refractive index is more important. The conductivity itself is certainly dependent on the frequency, but as long as we assume that the difference between the measured DC conductivity and the AC conductivity at

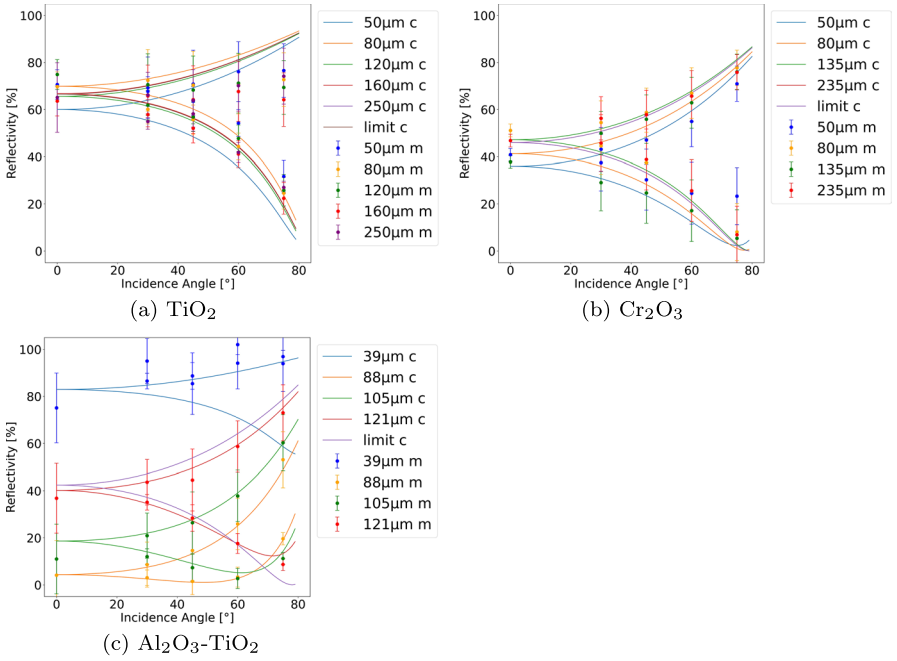

Fig. 8 The measured reflectivity dependent on the incidence angle. The upper curve of each color is the respective orthogonal polarization, the lower one the parallel. The dots with error bars represent the measurements, the lines the calculations. The calculations labeled with lines are the results for a very large thickness (5mm)

170GHz does not change over orders of magnitude, it still can be assumed that the imaginary part of the refractive index is the dominant contribution to the absorption coefficient for the compound material.

When comparing the values for the refractive index from Table 2 with literature values, 2.551 for Cr_2O_3 ([12]) and 2.61 for TiO_2 ([13]), the difference is a factor 2 and 4 respectively. There are two likely explanations for this: The main difference will be the vastly different frequencies measured, and refractive indices are in most cases simply not known for everything below the infared range, which still has frequencies at least a 100 times above the frequency of the measured microwaves. While it is challenging to predict the exact dependency of the refractive index on the frequency, it is not uncommon that it increases for lower frequencies. The second challenge for a comparison are the possible differences in the production process, which could lead to different modifications and surface properties.

7 Discussion

Coming back to the thickness dependency, two cases are not discussed yet, which can be predicted from the model, but no respective materials with the necessary low absorption coefficients were measured as part of this study. When decreasing

the absorption coefficient from the value of the compound material even more, we obtain the medium-low case, there the model shows a similar trend like the medium case - Al_2O_3-TiO_2 (Fig. 7e and f), with one notable exception: While the peak absorptivity still can reach almost 100%, for the thicknesses in between the peaks the absorptivity will almost completely go back to 0%. This is simply due to the fact that the absorption coefficient is now so low that a transmission through the layer without resonance leads to almost no absorption.

For extremely low absorption coefficients, even the absorptivity at the resonance starts to decrease rapidly because even with a high amount of reflections inside the layer, the material will simply not absorb much of the microwaves anymore.

This complicated dependency on the absorption coefficient leads to a rather unintuitive consequence: It is possible that using a material with a higher absorption coefficient as a layer microwave absorber actually leads to a decrease in absorptivity because a higher value can suppress the resonance effects, which lowers the amount of reflections inside the layer.

Another surprising effect can be noticed, when closer examining the position of the peak in absorption: The thickness, for which the peak occurs, is mostly independent of the incidence angle. Considering that this position comes from a phase shift and that the phase shift is dependent on the distance traveled through the layer, one would initially geometrically expect a bigger phase shift for higher incidence angles and thereby a shift of the position of the absorption peak to lower thicknesses. And this is actually the case (visible in Fig. 7e), but to a much lesser extent than expected. Two mechanisms are suppressing this effect: At first, as described in Section "2," not just the part of the wave, which moves through the layer experiences a phase shift, but also the part, which moves through air until the point, where it interferes with the first part. Because the phase shift outside of the layer is also bigger for bigger incidence angles and in the end just the difference between these phase shifts matter, this will decrease the angle dependency. The second mechanism is simply the high refractive index of all the measured materials, not a single one is estimated to be below 4. This leads to a much reduced transmission angle into the layer for every incidence angle, which leads to a comparable distance traveled inside the layer and thereby a reduced change in phase shift. Both of these mechanisms combined lead to the fact that the position (but not the value) of the peak of absorptivity is almost independent of the incidence angle, which is especially helpful, when trying to absorb isotropic stray radiation [11] .

For 90-μm and for 110-μm thicknesses of the compound material, two samples were prepared each under identical conditions. The reflectivity and the thickness measurements of these can give a good estimate of how well the production process is reproducible. While at nominally 90 μm (Al_2O_3-TiO_2-5 and Al_2O_3-TiO_2-6, see Table 1) the measured values are similar, there is a significant difference in thickness between the samples with nominally 110 μm (Al_2O_3-TiO_2-8 and Al_2O_3-TiO_2-9). This difference in thickness is inside the given error margin and the reflectivities exactly mirror the change in thickness as predicted by the model. The resulting difference in reflectivity is almost 10%, which comes from the fact that this thickness is close to the resonance. Thereby, it can be concluded that a maximal reflectivity

uncertainty of 10% must be expected when trying to design an absorber plate from the model data.

8 Conclusion

The production, measurement procedure, and modeling of three microwave absorbing materials are shown. By the sample preparation, it was shown that layers could be prepared reproducibly. Reflectivities of these layer materials at 170 GHz were then measured, dependent on thickness, polarization, and incidence angle. The model allowed to estimate the internal properties of the materials and also helped develop an understanding of the dependencies of the absorption, namely polarization, incidence angle, layer thickness, absorption coefficient, and refractive index. The model and the measurements were found to be in reasonable (>90%) agreement. Two surprising dependencies were observed and explained: That a higher absorption coefficient can actually lead to a decrease of absorption performance of the layer and that the position of the peak of absorption due to a resonance is almost independent of the incidence angle. Due to the high reliability of preparation, measurement, and modeling, it is reasonable to assume that microwave absorbing layer materials can be designed to fit the needs of future fusion reactors. To fit all future purposes, additional research is needed, especially in three areas: Firstly the yet mostly unknown, but vastly important, temperature dependency of the internal parameters ([14] shows the powers involved for dummy loads, [15] which changes can be expected from other MALMs). Secondly, a way to determine these internal parameters in a broad and continuous range during the production process, possibly by changing the percentages of Al_2O_3 and TiO_2 of the compound material [16]. Thirdly and finally, the exact frequency dependency of the internal parameters of these materials needs to be examined over a broader range (similar to [17]) inside the millimeter wave spectrum to be able to adapt to other gyrotron frequencies.

Acknowledgements At first, we want to thank the colleagues from ITER for the collaboration, in particular Melanie Preynas. Also a personal thanks to Achim Zeitler for the technical support. Moreover otherwise relevant is the support, which came in the form of the fruitful discussions with Walter Kasparek and Lina Wang.

Funding Open Access funding enabled and organized by Projekt DEAL.

Funding This work is supported by the Max Planck Institute for Plasma Physics (IPP), Garching and Greifswald.

Data Availability Data will be made available on reasonable request.

Declarations

Conflict of interest The authors declare no competing interests.

References

1. S.Gee et al., MAST neutral beam long pulse upgrade, Fusion Engineering and Design,74, 403-407 (2005), DOI:https://doi.org/10.1016/J.FUSENGDES.2005.06.094
2. P. van Eeten et al., W7-X NBI beam dump thermocouple measurements as safety interlock, Fusion Engineering and Design,146, 1329-1333 (2019), https://doi.org/10.1016/J.FUSENGDES.2019.02.069
3. W.Bin et al., Tests and developments of a long-pulse high-power 170 GHz absorbing matched load, Fusion Engineering and Design,146, 36-39 (2019), DOI:https://doi.org/10.1016/j.fusengdes.2018.11.019
4. Y.Duan and H.Guan, Microwave absorbing materials, Chapter 1, Pan Stanford Publishing Pte. Ltd., Singapore (2016)
5. Y.Q.Huang et al., Microwave absorbing materials: Solutions for real functions under ideal conditions of microwave absorption, Chinese Physics Letters, 27, 2 (2010), DOI:https://doi.org/10.1088/0256-307X/27/2/027702
6. W.Bin et al., Absorbing coatings for high power millimeter-wave devices and matched loads, Fusion Engineering and Design, 88, 2510-2514 (2013), DOI:https://doi.org/10.1016/j.fusengdes.2012.12.036
7. S.I.Alekseev and M.C.Ziskin, Reflection and absorption of millimeter waves by thin absorbing films, Bioelectromagnetics, 21, 264-271 (2000), https://doi.org/10.1002/(SICI)1521-186X(200005)21:4<264::AID-BEM3>3.0.CO;2-3
8. A.Killinger et al., Plasma spraying of a microwave absorber coating for an rf dummy load,Coatings, 11, 801 (2021), DOI:https://doi.org/10.3390/coatings11070801
9. I.Miccoli et al., The 100th anniversary of the four-point probe technique: the role of probe geometries in isotropic and anisotropic systems, Journal of Physics: Condensed Matter, 27, 223201 (2015), DOI:https://doi.org/10.1088/0953-8984/27/22/223201
10. A.Zavareh et al., Analysis of corrosion protection behavior of Al2O3-TiO2 oxide ceramic coating on carbon steel pipes for petroleum industry,Ceramics International, 44, 5967-5975 (2018), DOI:https://doi.org/10.1016/J.CERAMINT.2017.12.175
11. S.K.Nielsen et al., Strong scattering of mm-waves in tokamaks,Strong Microwaves and Terahertz Waves: Sources and Applications (2013)
12. M.MAbdullah et al.,Structural and optical characterization of Cr2O3 nanostructures: Evaluation of its dielectric properties (2014), DOI:https://doi.org/10.1063/1.4867012
13. DeVore, Refractive Indices of Rutile and Sphalerite,Journal of the Optical Society of America, (1951), DOI:https://doi.org/10.1364/JOSA.41.000416
14. J.W.Oosterbeek et al., Loads due to stray microwave radiation in ITER, Fusion Engineering and Design, 96-97, 553-556 (2015), DOI:https://doi.org/10.1016/j.fusengdes.2015.05.068
15. Z.Jia et al., ecent progresses of high-temperature microwave-absorbing materials,Nano, 13, 6 (2018), DOI:https://doi.org/10.1142/S1793292018300050
16. Z.Yang et al., Dielectric and microwave absorption properties of TiO2/Al2O3 coatings and improved microwave absorption by FSS incorporation, Journal of Alloys and Compounds, 678, 527 (2016), DOI:https://doi.org/10.1016/J.JALLCOM.2016.04.031
17. Z.Yang et al., Electromagnetic-wave absorption property of Cr2O3-TiO2 coating with frequency selective surface Synthesis and characterization of Perovskite and Spinel oxide films View project Material simulation View project Electromagnetic-wave absorption property of C, Journal of Alloys and Compounds, (2016), DOI:https://doi.org/10.1016/j.jallcom.2019.06.106